oxygen

MDPI

Article

Ginger-Derived Compounds Alleviate Oxidative Stress and Genotoxicity in *Trypanosoma evansi* Infection: An Integrated In Vivo and In Silico Study

Waqas Ahmad [1], Muhammad Yasin Tipu [1,*], Muti ur Rehman Khan [1], Haroon Akbar [2], Aftab Ahmad Anjum [3] and Muhammad Ovais Omer [4]

[1] Department of Pathology, Faculty of Veterinary Sciences, University of Veterinary and Animal Sciences, Lahore 54000, Pakistan; waqasahmadvet@gmail.com (W.A.); drniazi@uvas.edu.pk (M.u.R.K.)
[2] Department of Parasitology, Faculty of Veterinary Sciences, University of Veterinary and Animal Sciences, Lahore 54000, Pakistan; drharoonakbar@uvas.edu.pk
[3] Institute of Microbiology, Faculty of Veterinary Sciences, University of Veterinary and Animal Sciences, Lahore 54000, Pakistan; aftab.anjum@uvas.edu.pk
[4] Department of Pharmacology and Toxicology, Faculty of Biosciences, University of Veterinary and Animal Sciences, Lahore 54000, Pakistan; drovaisomer@uvas.edu.pk
* Correspondence: yasintipu@uvas.edu.pk; Tel.: +92-322-4027368

Abstract

Background/Objectives: *Trypanosoma evansi* (*T. evansi*) is an etiological agent of surra, and it causes significant economic losses in livestock. Rising trypanocide resistance demands alternatives that control parasitemia while mitigating oxidative and genotoxic damage. Therefore, the present study was designed to explore both the in vivo and in silico potential of *Zingiber officinale* (*Z. officinale*) as a novel phytotherapy to counter growing resistance against conventional trypanocides. Methods: Methanolic extract of *Z. officinale* (MZ) was orally administered at dosages of 200 mg/kg (MZ 200), 400 mg/kg (MZ 400), and 800 mg/kg (MZ 800) on a daily basis to the experimentally infected mice and compared against treated control (TC) and untreated control (UC) groups. After the infection, different parameters such as parasitemia counts, body weight changes, and the survival of infected mice were monitored for up to 7 days post-infection, while hematobiochemical parameters, oxidative stress profiles (catalase, malondialdehyde, and superoxide dismutase), and genotoxicity in brain tissues were compared at the end of the trial. Moreover, computational tools were used to predict the affinities of key bioactive compounds with twenty-one essential proteins of *T. evansi*. Results: The findings showed that the administration of MZ significantly ($p < 0.05$) reduced parasitemia and improved the survival rates in the experimentally infected mice in a dose-dependent manner. Noteworthy, significant ($p < 0.05$) improvements in hematological parameters and liver enzyme profiles were also recorded in MZ-treated groups. Compared to the untreated control, MZ-treated groups showed a significant amelioration in oxidative stress and genotoxicity in brain tissue in a dose-dependent fashion. The current study's findings suggest that MZ potentially inhibits various essential proteins of *T. evansi*, including adenosine transporter-1, casein kinase, leucyl-tRNA synthetase, and multidrug resistance E protein. Among its constituents, 6-Isoshogaol and 6-Gingerol showed the most stable interactions in the molecular dynamics simulation. Conclusions: MZ efficiently reduced parasitemia, oxidative stress, and genotoxicity, and increased the survival rate in infected mice, suggesting it as a promising natural trypanicidal agent.

check for updates

Academic Editor: John T. Hancock

Received: 9 July 2025
Revised: 26 August 2025
Accepted: 28 August 2025
Published: 1 September 2025

Citation: Ahmad, W.; Tipu, M.Y.; Khan, M.u.R.; Akbar, H.; Anjum, A.A.; Ovais Omer, M. Ginger-Derived Compounds Alleviate Oxidative Stress and Genotoxicity in *Trypanosoma evansi* Infection: An Integrated In Vivo and In Silico Study. *Oxygen* **2025**, *5*, 19. https://doi.org/10.3390/oxygen5030019

Keywords: *Trypanosoma evansi*; *Zingiber officinale*; methanolic extract; trypanicidal activity; molecular docking; bioactive compounds

1. Introduction

Pathogens pose a substantial threat to the health of humans, animals, and plants worldwide due to their vast diversity and high infectivity [1]. The effective prevention and treatment of these diseases remain significant medical challenges. Among these pathogens, *T. evansi* is a well-known blood protozoan responsible for surra in domestic animals [2]. This parasite affects a variety of species, including horses, buffaloes, cattle, and camels, leading to significant economic losses primarily due to animal mortality and decreased livestock productivity [3]. Atypical human infections with *T. evansi* have also been documented [4,5].

The treatment of surra primarily depends on trypanocides [6]. However, the emergence of drug-resistant trypanosomes has become a significant concern, leading to increased costs, reduced production efficiency, and a lack of effective control tools for farmers [7]. Commonly used anti-trypanosome drugs, such as melarsomine hydrochloride, suramin, quinapyramine, diminazene aceturate, and isometamidium chloride, have been used in field conditions for over thirty years [8].

However, researchers are exploring natural-resource-based therapies for more effective treatments due to the increasing resistance of parasites to existing therapeutics. Various compounds from medicinal plants have been reported to exhibit a wide range of pharmacological properties, including anti-inflammatory, antiprotozoal, immunomodulatory, and antibacterial effects [9,10]. *Z. officinale* (ginger) is a well-known spice with numerous pharmacological applications. It has traditionally been used as a household remedy to aid the digestive system and as an antiemetic [11]. Its bioactive components include volatile oils, gingerols, shogaols, paradols, gingerdiols, and zingerone. These compounds are responsible for anti-inflammatory, antiviral, antidiarrheal, antifungal, antibacterial, and antioxidant properties [12]. Additionally, various studies have described the antiparasitic potential of ginger against Trichinella spiralis, Schistosoma spp., microfilaria, Dirofilaria immitis, Toxoplasma gondii, and the hydatid cysts [13–17]. Previously, Kobo et al. [18] reported the efficacy of *Z. officinale* against *Trypanosoma brucei* in experimentally infected mice.

In addition to in vitro and in vivo experimentation, molecular docking studies and dynamic simulations may provide in-depth insights into the molecular mechanism of action of the bioactive phytochemical, identifying potential therapeutic targets [19]. Although *Z. officinale* has multifaceted pharmacological properties, which make it a promising alternative medicine, the specific mechanisms of action and its efficacy against T. evansi infections have not been fully explored to date. Despite its diverse pharmacological potential, it remains unclear whether *Z. officinale* bioactive compounds can alleviate the oxidative stress and genotoxic damage central to *T. evansi* pathology. Addressing this question is particularly important, given the limitations of existing trypanocides and the emerging crisis of resistance. The present study specifically investigates whether ginger-derived phytoconstituents can mitigate oxidative stress and genotoxicity, thereby offering mechanistic insights into their therapeutic potential against experimental *T. evansi* infection in mice.

2. Materials and Methods

2.1. Plant Extract Preparation and Phytochemical Profiling

The dried rhizome of *Z. officinale* was purchased from the local market in Lahore, Pakistan. Botanical identification was performed at the Botany Department, Government College University Lahore, Pakistan, and the plant specimen was submitted to the

herbarium (No. Gc. Herb. Bot. 4024). MZ was prepared by maceration as previously described [20]. The rhizome was ground to a fine powder, and approximately 300 g was macerated in 900 mL HPLC-grade methanol (Sigma Aldrich, Burlington, MA, USA, USA) for three days with repeated stirring to extract bioactive components as described by El-Kady et al. [21] with some modification. The extract was initially filtered through muslin-linen cloth and then through Whatman No.1 filter paper. The solvent was evaporated under reduced pressure at 40 °C. The dry extract was kept at 4 °C for the preparation of experimental doses.

The extract was analyzed by Gas Chromatography–Mass Spectrometry (GC-MS) using an Agilent 7890A GC system coupled with a 5975C mass spectrometer. Separation was achieved on a DB-5MS column (30 m × 0.25 mm, 0.25 µm). A 1 µL sample was injected with helium as the carrier gas (5:1) at 1 mL/min at 275 °C. The oven temperature started with 50 °C (2 min hold) and increased at 7 °C/min to 290 °C (1 min hold). The total run time was 37.286 min. The mass spectrometer was operated in scan mode over a m/z range of 35–500 [22].

2.2. Acute Toxicity Assay

The concentrated dried extract was dissolved in 2% Tween 80 for subsequent use in toxicity and pharmacological trials [18]. In the study, 18 mice were randomly allocated to six groups, each consisting of three mice. The groups were administered oral doses of 10 mg/kg, 100 mg/kg, 1000 mg/kg, 1500 mg/kg, 2000 mg/kg, and 3000 mg/kg with MZ. The subjects were observed for 24 h after the administration of doses regarding any mortality.

2.3. Isolation and Propagation of *T. evansi*

The blood obtained from the buffaloes (screened through Field's stained blood smear microscopy and PCR) was previously reported for *T. evansi* (NCBI accession No. PQ764013) [23]. The blood with the highest parasitemia was diluted using 1% chilled phosphate saline glucose and inoculated intraperitoneally in 6 rats (1 mL each) [18]. The rats were kept under standard housing and feeding conditions [24]. The presence and extent of parasitemia were assessed daily through the examination of blood smears for each animal. These blood smears from tail vein puncture were subjected to staining using the Field's stain and subsequently observed under a microscope. The parasites were counted in 10 fields at a magnification of 400×, as described by Herbert and Lumsden [25]. After the peak parasitemia, blood was collected and reconstituted in PSG to achieve the desired concentration (10^6 trypanosomes/mL).

2.4. Experimental Animals and Study Design

A total of twenty-five (n = 25) adult male mice were used in the experiment. The mice were kept in the research laboratory within the Department of Pathology for a 14-day acclimatization period, housed in standard hygienic conditions and accommodated in plastic cages furnished with wood shavings as bedding. The mice were kept in a controlled environment (24–26 °C), with a relative humidity level of 70–80%, a 12 h light period each day, and unrestricted access to feed and water [18]. The mice were randomly assigned to five groups, with five mice in each group. All of the groups were intraperitoneally infected with 100 µL of *T. evansi*-infected blood from rats at an approximate concentration of 10^6 trypanosomes/mL.

Groups I-III received MZ orally (reconstituted in Tween 80) at the dose rate of 200 mg/kg (MZ 200), 400 mg/kg (MZ 400), and 800 mg/kg (MZ 800) body weight once daily, respectively, for seven days, following Kobo et al. [18]. Group IV was injected with a single dose of isometamidium chloride (1 mg/kg) intraperitoneally as a positive control

(treated control). Group V was administered orally Tween 80 (1 mL/kg) once daily to serve as a negative control (untreated control). Mortality was observed, and parasitemia was recorded daily from tail vein blood using the rapid matching method described previously by Herbert and Lumsden [25]. Body weight was recorded daily using a digital weighing balance and mortality was observed daily. Blood was collected aseptically through cardiac puncture under anesthesia (5% Ketamine Hydrochloride at a dosage of 22 mg/kg body weight injected intramuscularly) [26]. Blood samples were taken in vacutainers with and without anticoagulants for hematobiochemical analysis [27]. After the blood sample collection, the mice were subjected to euthanasia through decapitation [28]. These brain samples were then dissected in duplicates on a glass dish placed over ice to prepare for the measurement of oxidative stress and genotoxic parameters, respectively. Brain tissue samples were collected and immediately stored at −80 °C until processing. The malondialdehyde (MDA) levels in brain tissue were estimated through colorimetric procedures of thiobarbituric acid [29] and a commercial kit (CAT100-1KT, Sigma-Aldrich®, St. Louis, MI, USA), respectively. The tissue was weighed and homogenized in chilled phosphate-buffered saline (pH 7.4). A 1:10 (w/v) dilution was prepared by adding 9 mL of buffer per 1 g of tissue using a homogenizer. The homogenate was centrifuged at 10,000× g for 10–15 min at 4 °C to collect the supernatant for further analysis [30]. Briefly, 200 µL of tissue supernatant was mixed with 800 µL of TBA-TCA reagent. The mixture was heated in a boiling water bath at 95 °C for 30–60 min. After cooling, the mixture was centrifuged at 3000× g for 10 min. The absorbance of the supernatant was measured at 532 nm using a spectrophotometer [29].

For estimation of catalase (CAT) activity, a combination of 50 µL of newly made 20 mM H_2O_2, 50 µL of 50 mM phosphate buffer (pH 7), and 20 µL of tissue homogenate supernatant was used to measure CAT activity in microplate wells. The decrease in absorbance resulting from H_2O_2 breakdown was measured over three minutes at 240 nm using a microplate reader spectrophotometer. A 39.4 mM^{-1} cm^{-1} extinction coefficient was used to assess CAT activity, which was then expressed as nmol of H_2O_2 destroyed per minute per milligram of protein [31,32]. Superoxide dismutase (SOD) levels in brain tissue were estimated using a commercial kit (Catalogue no: 19610-1KT-F, Sigma-Aldrich, St. Louis, MI, USA). Preparation of a single-cell suspension from organs was carried out according to the method of Tice et al. [21]. To assess genotoxicity, the alkaline comet assay was conducted following the alkaline method [33]. OpenComet v1.3 software for Windows was used to evaluate the tail length of the comet. The genetic damage index was estimated using the formula described by Ahmad et al. [34].

$$\frac{(No.of\ cells\ in\ class\ I) + (2\ \times\ No.of\ cells\ in\ class\ II) + (3\ \times\ No.of\ cells\ in\ class\ III) + (4\ \times\ No.of\ cells\ in\ class\ IV)}{\text{No.of cells in class 0} + \text{No.of cells in class I} + \text{No.of cells in class II} + \text{No.of cells in class III} + \text{No.of cells in class IV}}$$

2.5. Ligand Preparation

In the present study, the 3D structures of the active phytochemicals from GC-MS analysis of MZ were retrieved in structure-data file format from PubChem (https://pubchem.ncbi.nlm.nih.gov/ (accessed on 24 October 2024)). The LigPrep module in the Schrödinger suite (Maestro 14.0) was employed for the preparation of ligands. Optimized potentials for liquid simulation, 4 force field, and Epik (target pH: 7.0 ± 2.0) methods were used to generate multiple ionization states of the ligands.

2.6. Protein Sequence Retrieval and Homology Modeling Proteins

Twenty-one essential proteins of *T. evansi* were selected after a comprehensive literature review, focusing on their critical roles in cellular metabolism and survival. The complete gene sequences for adenosine transporter-1 (TbAT1), alternative oxidase, aquaglyceroporin, arginine kinase, ATP synthase subunit beta, beta-tubulin, calcium transporting ATP-ase, casein kinase, cytochrome C oxidase subunit-IV, glycerol kinase,

haptoglobin hemoglobin receptor, hexokinase, leucyl t-RNA synthetase, mismatch repair ATPase, multidrug resistance protein E, oligopeptidase B, ribonucleotide reductase large subunit, telomerase reverse transcriptase, topoisomerase-II, trans-sialidase, and trypanothione reductase were retrieved in FASTA format from the NCBI database (http://www.ncbi.nlm.nih.gov/ (accessed on 24 October 2024)). Gene translation was conducted using ExPASy (https://web.expasy.org/translate/ (accessed on 24 October 2024)). The three-dimensional structures of the proteins were constructed using SWISS-MODEL (https://swissmodel.expasy.org/ (accessed on 25 October 2024)). The stereochemical properties of these modeled proteins were analyzed by Ramachandran plots [35]. Overall model quality and 3D structural evaluation were performed using ERRAT [36] and VERIFY-3D accessed through the SAVES v6.1 web server (https://saves.mbi.ucla.edu/ (accessed on 25 October 2024)). The physicochemical properties of the modeled proteins were checked at ProtParam (https://web.expasy.org/protparam/ (accessed on 27 October 2024)) [37].

2.7. Protein Preparation, Site Map Analysis, Receptor Grid Generation, Ligand Docking, and Free Energy Calculation

Preprocessing was carried out using the Protein Preparation Wizard within the Schrödinger suite (Maestro 14.0) [38]. The selected proteins were subjected to binding-site analysis with the SiteMap module of the Maestro 14.0 (Schrödinger suite 2024-2) [39]. A receptor grid was generated with the receptor grid generation tool. Ligands were then used for high-throughput virtual screening, standard precision Glide docking, and extra precision (XP) Glide docking through flexible docking mode [40]. The Glide GScore was calculated using the formula:

$$GScore = a \times vdW + b \times Coul + Lipo + H - bond + Metal + BuryP + RotB + site$$

where vdW is van der Waals energy, Coul is Coulomb energy, Lipo is lipophilic contact, H-bond represents hydrogen bonding, Metal shows metal binding, BuryP describes the penalty for buried polar groups, RotB is the penalty for freezing rotatable bonds, and site denotes polar interactions in the active site. The coefficients for vdW and Coul in the equation are a = 0.065 and b = 0.130, respectively [41]. Following docking, the Prime MM-GBSA module in the Schrödinger suite 2024-2 was used to calculate the binding free energies of the protein-ligand complexes [42].

2.8. ADMET Analysis

To verify the potential of phytochemicals in revealing significant interactions with *T. evansi* proteins as effective drug candidates, ADMET analysis was performed using the QikProp module [43].

2.9. Molecular Dynamic Simulations

The stability of the coupled [6]-Isoshogaol and TbAT1 complex was assessed through a 50 ns molecular dynamics (MD) simulation analysis. The complex in the explicit solvent system utilizing the OPLS4 force field was analyzed using the Desmond module of Schrödinger 2024-2. The molecular system was solubilized using crystallographic water (TIP5P) molecules within orthorhombic periodic boundary conditions, utilizing a 10 Å buffer zone. The redundant water molecules were removed, and the system was neutralized by including Na^+ ions. An NPT ensemble and barostat were utilized to sustain a constant temperature of 300 K and pressure of 1 bar in the systems, respectively. The results were recorded at intervals of 50 picoseconds, and the resulting trajectory was analyzed using the Maestro 14.0 graphical interface.

2.10. Statistical Analysis

The data was initially compiled in Microsoft Excel (version 16.0.17928). The survival of the experimental mice was analyzed by using the Kaplan–Meier model. The trypomastigote count (per μL/blood) and body weight on a daily basis were compared among the groups using two-way ANOVA followed by post hoc multiple comparison with Sidak correction. Hematobiochemical parameters, oxidative stress markers, and GDI were compared using one-way ANOVA and Tukey's post hoc test. Descriptive statistics and the Chi-square test were used to analyze the frequencies of various cell classes from the comet assay using Minitab software (version 21.4.2). Graphs were generated using GraphPad Prism (version 9.5.0).

3. Results

3.1. Phytochemical Profiling

Briefly, 20 phytochemicals were detected in MZ through GC-MS analysis. 1-(4-Hydroxy-3-methoxyphenyl)oct-4-en-3-one accounted for 17.53. The major constituents included (4S)-1-methyl-4-(6-methylhepta-1,5-dien-2-yl)cyclohexene (10.31%), 1-(4-Hydroxy-3-methoxyphenyl)dodec-4-en-3-one (6.67%), and N-[(4-hydroxy-3-methoxyphenyl)methyl]-8-methylnonanamide (7.54%). Other significant compounds included 1-(4-Hydroxy-3-methoxyphenyl)tetradec-4-en-3-one (9.42%), 1-(4-Hydroxy-3-methoxyphenyl)tetradecane-3,5-dione (4.27%) and [(5S)-1-(4-hydroxy-3-methoxyphenyl)-3-oxodecan-5-yl] acetate(3.61%). Comparatively lower concentrations of N-[(4-hydroxy-3-methoxyphenyl)methyl]-9-methyldecanamide (3.55%), [[C-(4-chlorophenyl)-N-ethylcarbonimidoyl]amino] benzoate (3.03%), and 2,3,4,6-tetrahydro-1,6-benzoxazocin-5-one (2.25%) were found. The compounds such as hexadecanoic acid (2.92%) and (E)-1-(4-Hydroxy-3-methoxyphenyl)tetradec-3-en-5-one (2.71%) were also detected. Additionally, (E)-1-(4-Hydroxy-3-methoxyphenyl)dec-3-en-5-one was present at 1.75% (Table 1).

Table 1. GC-MS profiling of methanolic extract of Zingiber officinale revealing phenolic and hydrocarbon compounds.

Peak	IUPAC Name	Common Name	Retention Time (min)	Area %	PubChem CID
1	1-methyl-4-(6-methylhept-5-en-2-yl)benzene	alpha-Curcumin	10.118	7.71	92139
2	2-methyl-5-(6-methylhept-5-en-2-yl)cyclohexa-1,3-diene	l-Zingiberene	10.235	10.31	521253
3	(4S)-1-methyl-4-(6-methylhepta-1,5-dien-2-yl)cyclohexene	beta-Bisabolene	10.337	4.52	10104370
4	3-(6-methylhept-5-en-2-yl)-6-methylidenecyclohexene	Sesquiphellandrene	10.492	5.3	519764
5	4-(4-hydroxy-3-methoxyphenyl)butan-2-one	Zingiberone	11.476	2.19	31211
6	1-cyclopropylethyl N-phenylcarbamate	1-Cyclopropylethyl phenylcarbamate	11.878	2.46	263797
7	2,3,4,6-tetrahydro-1,6-benzoxazocin-5-one	2H-1,6-Benzoxazocin-5(6H)-one,3,4-dihydro	12.717	2.25	550286
8	hexadecanoic acid	Palmitic acid	13.717	2.92	985
9	1-(3-methoxy-4-propan-2-yloxyphenyl)propan-2-one	Propan-2-one,1-(4-isopropoxy-3-methoxyphenyl)-	14.707	1.57	586436
10	2-[bis(2-hydroxyethyl)amino]ethanol; (9Z,12Z)-octadeca-9,12-dienoic acid	Linoleic acid	14.851	0.7	5280450
11	(E)-1-(4-Hydroxy-3-methoxyphenyl)dec-3-en-5-one	6-Isoshogaol	15.413	1.75	11694761

Table 1. *Cont.*

Peak	IUPAC Name	Common Name	Retention Time (min)	Area %	PubChem CID
12	1-(4-Hydroxy-3-methoxyphenyl)oct-4-en-3-one	1-(4-Hydroxy-3-methoxyphenyl)oct-4-en-3-one	15.91	17.53	71357126
13	N-[(4-hydroxy-3-methoxyphenyl)methyl]-8-methylnonanamide	Dihydrocapsaicin	16.119	7.54	107982
14	[[C-(4-chlorophenyl)-N-ethylcarbonimidoyl]amino] benzoate	O-Benzoyl-4-chloro-N-ethylbenzamidoxime	16.927	3.03	586265
15	1-(4-Hydroxy-3-methoxyphenyl)dodec-4-en-3-one	8-Shogaol	17.023	6.67	6442560
16	[(5S)-1-(4-hydroxy-3-methoxyphenyl)-3-oxodecan-5-yl] acetate	6-Gingerol monoacetate	17.216	3.61	91715794
17	(E)-1-(4-Hydroxy-3-methoxyphenyl)tetradec-3-en-5-one	10-Isoshogaol	17.702	2.71	53379231
18	1-(4-Hydroxy-3-methoxyphenyl)tetradec-4-en-3-one	-	18.13	9.42	181491
19	N-[(4-hydroxy-3-methoxyphenyl)methyl]-9-methyldecanamide	Homodihydrocapsaicin-I	18.285	3.55	3084336
20	1-(4-Hydroxy-3-methoxyphenyl)tetradecane-3,5-dione	10-Gingerdione	18.328	4.27	14440539

3.2. Acute Toxicity Assay

None of the mice died within 24 h after treatment with the MZ at dose rates of up to 3000 mg/kg.

3.3. Effect of Treatment on Survival of Infected Mice

No mortality was observed in any group until 3 DPI. Afterwards, the results were suggestive of the dose-dependent effects of MZ regarding survival. Kaplan–Meier survival analysis curve revealed a significant difference in survival probability between the treatment groups ($\chi^2 = 5.890$, df = 1, $p < 0.05$). No mortality was observed in the positive control and the MZ 800-treated groups. In contrast, the negative control and MZ 200 and MZ 400 groups exhibited a progressive decrease in survival, particularly after four days post-infection. Each group consisted of five individual mice ($n = 5$), and the survival and parasitemia outcomes were reported based on these biological replicates (Figure 1).

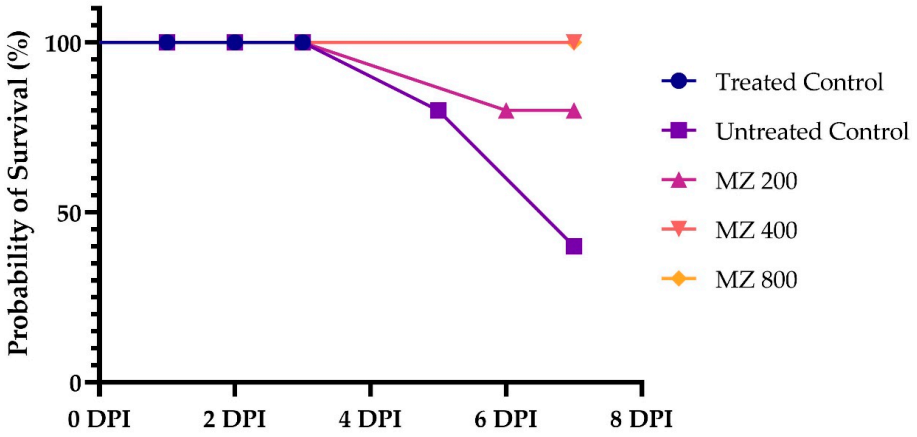

Figure 1. Survival probability of mice treated with MZ at 200 mg/kg, 400 mg/kg, and 800 mg/kg compared to treated and untreated controls over 7 days post-infection (DPI). Survival curves for the treated control and MZ800 groups overlapped with MZ400, as no mortality was observed in these groups. Data represent survival outcomes for $n = 5$ mice per group.

3.4. Comparison of Parasitemia

Comparison of the parasitemic loads revealed significant ($p < 0.05$) differences among the treatment groups. At 1 DPI, none of the groups showed trypanosomes in the wet smear. However, on day 2, DPI showed a few trypomastigotes that could only be observed in the untreated control. Conversely, the positive control group did not develop the infection until the end of the experiment. MZ-treated groups revealed significantly lower parasitemic count compared with the untreated control each day in a dose-dependent manner. At 7-DPI, the significantly highest mean parasitemic count (4.42×10^5 µL) was recorded in the untreated control, followed by the MZ 200 (3.63×10^5 µL) and MZ 400 (3.52×10^5 µL) groups, which did not vary significantly from each other. However, the MZ 800-treated group showed a significantly lower mean trypomastigote count (3.04×10^5 µL) than the untreated control and MZ 200- and MZ 400-treated groups (Figure 2).

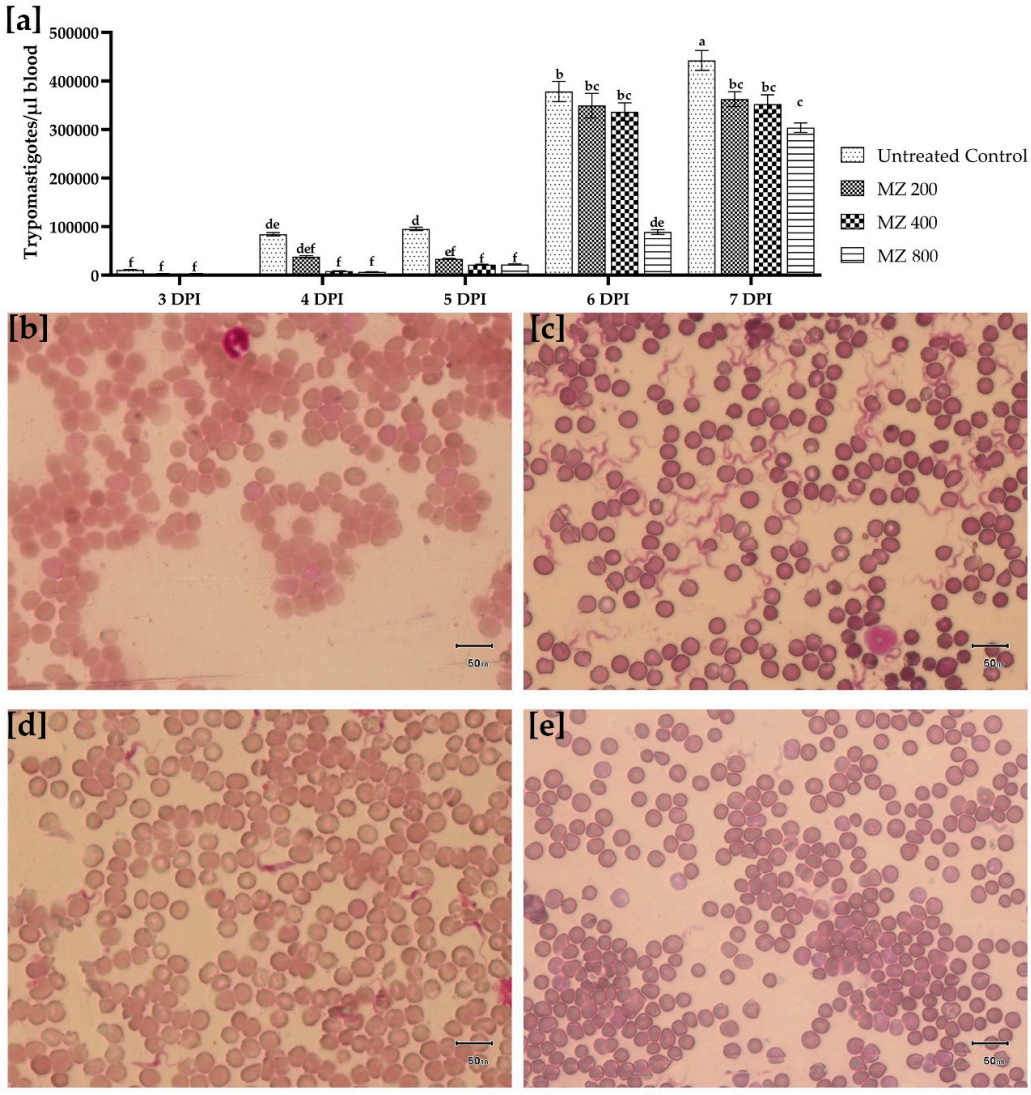

Figure 2. (**a**) Comparison of *T. evansi* trypomastigotes quantification in the blood at various days post-infection for untreated control, MZ 200 mg/kg, MZ400 mg/kg, and MZ800 mg/kg treated groups. Data is presented as mean (±S.E.M), with different superscript letters (a, b c, d, e and f) showing the means are differing significantly ($p < 0.05$). Field's-stained thin blood smears prepared showing (**b**) absence of parasitemia in isometamidium chloride treated control group (1 mg/kg single intraperitoneal dose), (**c**) high parasitemia load in untreated control group, (**d**) comparatively low trypomastigote count in MZ 200 mg/kg treated group, and (**e**) least trypomastigote count observed per microscopic field in MZ 800 mg/kg treated group at 7 days post-infection (40×).

3.5. Impact of Treatment of Body Weight

The body weight comparison across groups at baseline revealed no significant differences in the body weight of the positive control, untreated control, and treatment groups (MZ 200, MZ 400, and MZ 800). However, at 7 dpi, a decline in body weight was evident in the untreated control and lower-dose groups (MZ 200 and MZ 400). In contrast, the MZ 800 group showed more consistent maintenance of body weight, comparable to the positive control group. In contrast, the untreated control group exhibited a significant ($p < 0.05$) reduction in body weight (Figure 3).

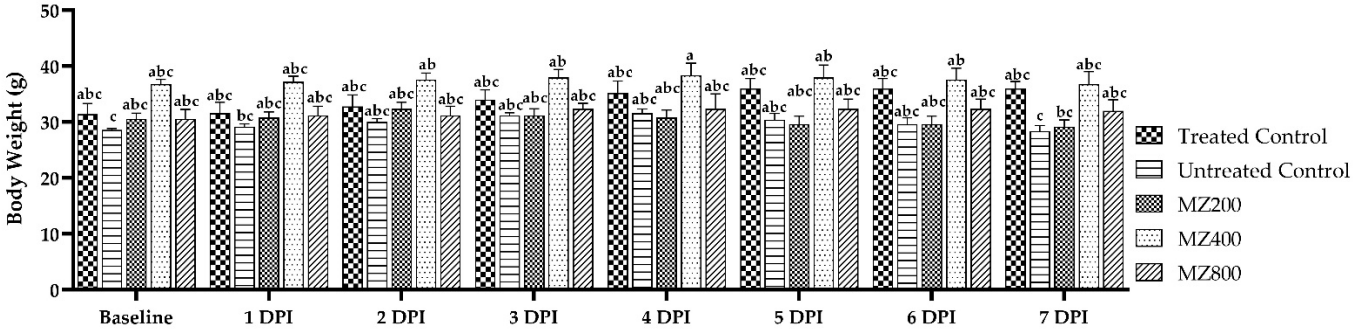

Figure 3. Comparison of mice's body weight measurements (g) from baseline to 7 days post-infection with *T. evansi*, for the treated control, untreated control, and MZ 200-, MZ 400-, and MZ 800-treated groups. Significant differences ($p < 0.05$) among the means are indicated by different superscripts different superscript letters (a, b and c) over the standard error of mean bars.

3.6. Hematobiochemical Changes

The results revealed significant differences ($p < 0.05$) in hematological and biochemical parameters among the groups. The mean hemoglobin (Hb) and total erythrocyte counts (RBC) were significantly ($p < 0.05$) higher in the positive control group (10.9 g/dL and 8.06 $\times$ 10^6 µL), followed by MZ 800 (10.1 g/dL and 7.81 $\times$ 10^6 µL), compared with MZ 200, MZ 400, and the untreated control. The total leukocyte counts (TLC) were significantly ($p < 0.05$) higher in the untreated control (8.05 $\times$ 10^3 µL) and significantly ($p < 0.05$) lower in the positive control (4.74 $\times$ 10^3 µL), followed by the MZ 800 (5.23 $\times$ 10^3 µL) group. Additionally, the treated control (32.9 g/dL) revealed the highest MCHC levels (g/dL), followed by MZ 800 (31.3 g/dL). However, no significant ($p > 0.05$) difference could be observed regarding mean hematocrit (Hct %), mean corpuscular hemoglobin (MCH pg) levels, and platelet count ($\times 10^3$ µL) between the groups. Furthermore, differential leukocyte count did not show significant differences in relative percentages of neutrophil, lymphocyte, monocyte, and eosinophil across groups. Moreover, the comparison of bilirubin levels did not show significant changes across all groups. Alanine transaminase (ALT) and aspartate transaminase (AST) levels were significantly elevated in the untreated control (133 mg/dL and 278 mg/dL, respectively). Conversely, significantly lower levels were seen in the treated control (53.5 mg/dL and 133 mg/dL, respectively), followed by MZ 800 (ALT; 65.7 mg/dL and AST; 107 mg/dL). Similarly, total protein was also significantly elevated in the treated control, followed by MZ 800. However, the A/G ratio was highest in MZ 200 (0.903 $\pm$ 0.0393) compared to the treated control, which showed the lowest levels. Overall, MZ 800 revealed significant improvement in hematobiochemical profiles comparable with the treated control in contrast with the lower MZ doses and untreated control (Table 2). These hematobiochemical improvements, particularly in Hb, RBC, and liver enzyme profiles, are not only indicative of reduced disease pathology but also align with the attenuation of oxidative stress responses observed in the infected mice.

Table 2. Hematological and biochemical parameters in untreated control, treated control, and MZ-treated groups at different doses (200 mg/kg, 400 mg/kg, and 800 mg/kg). Parameters include hemoglobin (Hb), red blood cell count (RBC), total leukocyte count (TLC), hematocrit (Hct), mean corpuscular volume (MCV), mean corpuscular hemoglobin (MCH), mean corpuscular hemoglobin concentration (MCHC), platelet count, and differential leukocyte counts (neutrophils, lymphocytes, monocytes, eosinophils), along with liver function markers (bilirubin, ALT, AST), and protein levels (total protein, albumin, globulin, and A/G ratio). Values are presented as mean ± SEM. Different superscript letters (^{a}, ^{b}, ^{c}, ^{d} and ^{e}) indicate significant ($p < 0.05$) differences between group means.

Parameter	Untreated Control	Treated Control	MZ 200	MZ 400	MZ 800
Hb (gm/dL)	9.18 ± 0.0666 ^{b}	10.9 ± 0.507 ^{a}	9.11 ± 0.0321 ^{b}	9.39 ± 0.0825 ^{b}	10.1 ± 0.0371 ^{ab}
RBCs ($\times 10^6$ µL)	7.23 ± 0.0346 ^{c}	8.06 ± 0.0636 ^{a}	7.27 ± 0.0536 ^{c}	7.34 ± 0.0644 ^{c}	7.81 ± 0.0173 ^{b}
TLC ($\times 10^3$ µL)	8.05 ± 0.319 ^{a}	4.74 ± 0.169 ^{c}	6.05 ± 0.147 ^{b}	5.18 ± 0.0318 ^{c}	5.23 ± 0.0667 ^{bc}
Hct (%)	32.6 ± 0.583	33.1 ± 0.468	32.5 ± 0.426	32.8 ± 0.436	32.4 ± 0.434
MCV (fl)	45.1 ± 0.637 ^{a}	41 ± 0.535 ^{b}	44.7 ± 0.382 ^{a}	44.7 ± 0.224 ^{a}	41.4 ± 0.483 ^{b}
MCH (pg)	12.7 ± 0.149	13.5 ± 0.643	12.5 ± 0.122	12.8 ± 0.0617	13 ± 0.0713
MCHC (g/dL)	28.2 ± 0.682 ^{bc}	32.9 ± 1.15 ^{a}	28 ± 0.455 ^{c}	28.6 ± 0.179 ^{bc}	31.3 ± 0.465 ^{ab}
Platelets ($\times 10^3$ µL)	348 ± 10.4	382 ± 2.56	341 ± 34.2	382 ± 28.2	394 ± 2.02
Neutrophil (%)	25 ± 2.11	21.5 ± 0.582	24.5 ± 2.23	22.4 ± 0.726	23.7 ± 0.287
Lymphocyte (%)	69.7 ± 2.36	73.9 ± 0.214	70.8 ± 2.36	73.4 ± 1.23	71.3 ± 0.415
Monocyte (%)	3.68 ± 0.354	3.11 ± 0.479	3.31 ± 0.663	2.89 ± 0.496	3.28 ± 0.49
Eosinophil (%)	1.64 ± 0.157	1.54 ± 0.223	1.45 ± 0.144	1.31 ± 0.11	1.71 ± 0.151
Bilirubin (mg/dL)	0.31 ± 0.05	0.293 ± 0.0433	0.32 ± 0.0416	0.333 ± 0.0524	0.337 ± 0.0448
ALT (mg/dL)	133 ± 1.59 ^{a}	53.5 ± 1.84 ^{e}	107 ± 1.99 ^{b}	89.9 ± 0.361 ^{c}	65.7 ± 2.4 ^{d}
AST (mg/dL)	278 ± 2.02 ^{a}	133 ± 1.82 ^{c}	152 ± 1.68 ^{b}	135 ± 1.34 ^{c}	107 ± 0.936 ^{d}
Total Proteins (u/L)	5.32 ± 0.0874 ^{e}	8.61 ± 0.111 ^{a}	6.03 ± 0.0984 ^{d}	6.88 ± 0.231 ^{c}	7.89 ± 0.102 ^{b}
Albumin (u/L)	2.32 ± 0.0285 ^{d}	3.42 ± 0.0557 ^{a}	2.86 ± 0.0208 ^{c}	3.16 ± 0.0203 ^{b}	3.3 ± 0.024 ^{ab}
Globulin (u/L)	3 ± 0.1 ^{d}	5.2 ± 0.0677 ^{a}	3.17 ± 0.115 ^{cd}	3.72 ± 0.212 ^{c}	4.59 ± 0.0929 ^{b}
A/G Ratio	0.777 ± 0.0296 ^{ac}	0.66 ± 0.01 ^{c}	0.903 ± 0.0393 ^{a}	0.857 ± 0.0433 ^{ab}	0.72 ± 0.0115 ^{bc}

3.7. Oxidative Stress and Genotoxicity in Brain Tissue

The analysis of oxidative stress markers in brain tissue of the experimentally infected mice revealed that CAT activity was significantly higher (16.6 ± 0.685 U/L) in the TC group compared to the UC group (9.39 ± 0.505 U/L), all MP-treated groups, and lower doses of MZ (200 and 400 mg/kg). However, the MZ 800 treatment led to a moderate but significant increase in CAT activity (13.1 ± 0.12 U/L), showing a dose-dependent improvement in antioxidant defense. For MDA, the TC group showed the highest levels (2.87 ± 0.13 µmol/L), whereas the UC group had the lowest (0.56 ± 0.15 µmol/L). Notably, MZ at 400 mg/kg brought about a significant reduction in MDA (1.92 ± 0.065 µmol/L), and MZ at 800 mg/kg showed an even stronger effect (1.31 ± 0.1 µmol/L) and indicated a clear dose-dependent protective response. SOD activity was the highest in the TC group (16.8 ± 0.15 U/mg), and the UC group had significantly ($p < 0.05$) lower levels (6 ± 0.27 U/mg) (Table 3).

Comparison of the comet assay of brain tissues from the mice of experimental groups revealed that the TC group had a significantly (χ^2 169.302, df; 28, $p < 0.0001$) higher proportion of Class 0 cells (69.39%). However, a significant portion still showed early to moderate damage (19.39% Class 1, 8.16% Class 2, and 3.06% Class 3 cells). Moreover, having a high percentage of undamaged cells, this group had the shortest tail length (6.41 ± 0.683 µm) and the lowest GDI (0.306 ± 0.0204). The UC group showed a higher proportion of cells with genetic damage. Tail lengths of the comets were longer in this group (15 ± 1.16 µm), and the GDI was higher (0.83 ± 0.01). The proportion of Class 3 and Class 4 cells was higher in the MP-treated groups (200, 400, and 800 mg/kg). The GDI values were statistically comparable ($p > 0.05$) to those of the UC group. On the other hand, at MZ 200, there was a mild but non-significant reduction in DNA damage (GDI; 0.771) and tail length (13.7 ± 1.12 µm). Moreover, the genoprotective effect was more noticeable

at MZ 800, where the percentage of undamaged cells (Class 0) was recorded as 39.36%, tail length was 9.89 ± 1.02 µm, and the GDI was 0.606 ± 0.0319 (Figure 4).

Table 3. Comet assay analysis showing the percentage distribution of DNA damage classes (Class 0–4), tail length (µm), and Genotoxic Damage Index (GDI) in brain tissue of mice from different experimental groups. The proportion of cell types was compared using the Chi-square test, while the tail length and GDI were compared through one-way ANOVA and Tukey's post-hoc test. Different superscript letters (^{a}, ^{b}, ^{c}, ^{d} and ^{e}) indicate significant ($p < 0.05$) differences between group means. Statistically significant differences were considered significant at $p < 0.05$.

Group	TC	UC	MZ 200	MZ 400	MZ 800
CAT (U/L)	16.6 ± 0.685 ^{a}	9.39 ± 0.505 ^{c}	9.14 ± 0.125 ^{c}	9.43 ± 0.005 ^{c}	13.1 ± 0.12 ^{b}
MDA (µmol/L)	0.56 ± 0.15 ^{d}	2.87 ± 0.13 ^{a}	2.88 ± 0.01 ^{a}	1.92 ± 0.065 ^{b}	1.31 ± 0.1 ^{c}
SOD (U/mg)	16.8 ± 0.15 ^{a}	6 ± 0.27 ^{de}	7.46 ± 0.425 ^{d}	9.14 ± 0.465 ^{c}	12.6 ± 0.26 ^{b}
Class 0	69.39% (59.68–77.64)	17% (10.89–25.55)	23% (15.84–32.15)	27.72% (19.93–37.15)	39.36% (30.09–49.47)
Class 1	19.39% (12.78–28.31)	33% (24.56–42.69)	32% (23.67–41.66)	31.68% (23.42–41.29)	36.17% (27.18–46.25)
Class 2	8.16% (4.19–15.29)	37% (28.18–46.78)	34% (25.46–43.72)	32.67% (24.31–42.31)	18.09% (11.61–27.07)
Class 3	3.06% (0.83–8.62)	10% (5.52–17.44)	8% (4.11–15)	4.95% (2.13–11.07)	4.26% (1.67–10.44)
Class 4	0% (0–3.77)	3% (0.82–8.45)	3% (0.82–8.45)	2.97% (0.81–8.37)	2.13% (0.38–7.43)
Tail Length (µm)	6.41 ± 0.683 ^{c}	15 ± 1.16 ^{a}	13.7 ± 1.12 ^{ab}	13.1 ± 1.12 ^{ab}	9.89 ± 1.02 ^{bc}
GDI	0.306 ± 0.0204 ^{e}	0.83 ± 0.01 ^{ac}	0.771 ± 0.0254 ^{bc}	0.723 ± 0.0225 ^{cd}	0.606 ± 0.0319 ^{d}

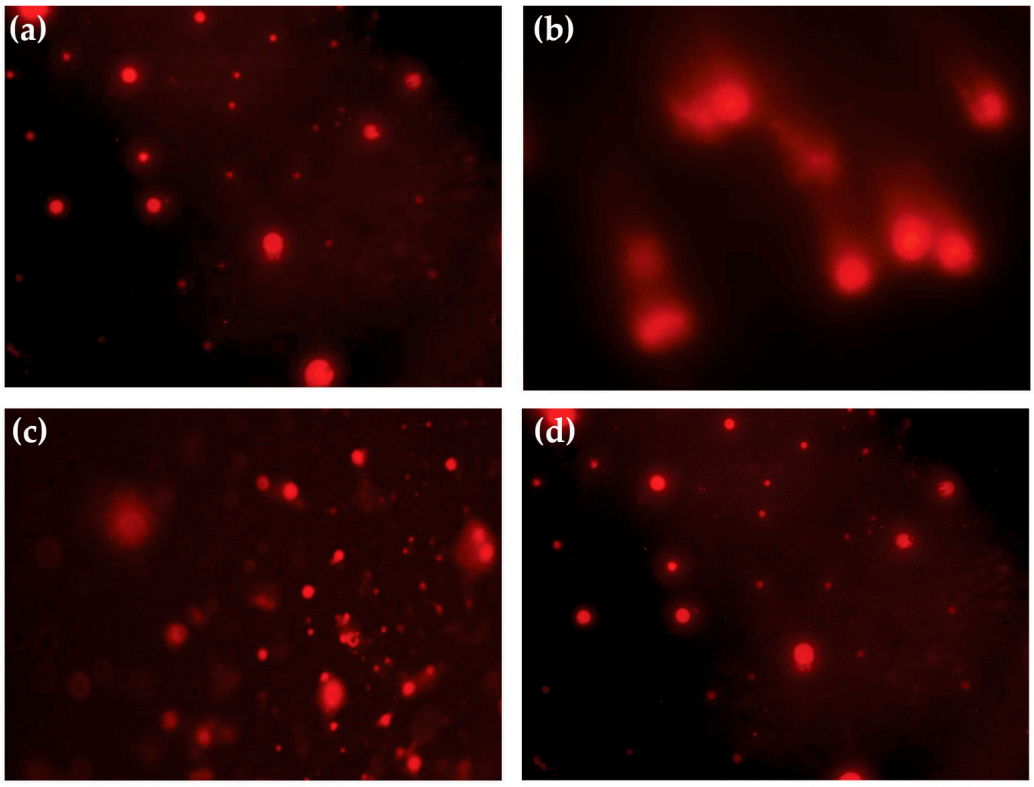

Figure 4. Representative comet assay images depicting DNA damage in blood lymphocytes of *T. evansi*-infected mice observed under a fluorescence microscope. (**a**) TC (treated control); (**b**) UC (untreated control); (**c**) MZ 200 mg/kg; and (**d**) MZ 800 mg/kg treated groups.

3.8. Ligand Docking and Free Binding Energy Calculations

The results of glide docking and MM-GBSA analysis revealed the strongest binding affinity of [6]-Isoshogaol with TbAT1 (XP GScore; −9.18309 and MMGBSA dG Bind;

−68.7548), followed by 8-Shogaol (glide emodel; −48.1948 and MMGBSA dG Bind; −69.8895). In contrast, the affinity of 2,3,4,6-tetrahydro-1,6-benzoxazocin-5-one was comparatively weaker (XP GScore of −8.07276 and MMGBSA dG Bind of −40.3092). Moreover, 1-(4-Hydroxy-3-methoxyphenyl) oct-4-en-3-one showed favorable affinity (MMGBSA dG Bind; −68.2929 and glide emodel; −39.9705) against casein kinase. On the other hand, zingerone showed a favorable interaction with leucyl-tRNA synthetase (MMGBSA dG Bind; −50.9063). Additionally, 8-Shogaol also showed significantly strong affinity to multidrug resistance protein E (glide emodel; −46.2196 and MMGBSA dG bind; −79.0799). Collectively, [6]-Isoshogaol and 8-Shogaol were identified as the most promising drug candidates based on their consistent favorable binding energies (Table 4).

Table 4. Molecular docking and binding free energy analysis of ginger-derived compounds against four target proteins (adenosine transporter 1, casein kinase, leucyl tRNA synthetase, and MRP E). The glide model, XP GScore, and MM-GBSA binding energies (total dG Bind, Coulomb, lipophilic (Lipo), and van der Waals (vdW) contributions) are presented. Compounds exhibited favorable docking scores and binding affinities, with the van der Waals component being the primary contributor to the total binding energy.

Ligand Pubchem CID	Protein	Glide Emodel	XP GScore	MMGBSA dG Bind(NS)	MMGBSA dG Bind(NS) Coulomb	MMGBSA dG Bind(NS) Lipo	MMGBSA dG Bind(NS) vdW
11694761	TbAT1	−47.0134	−9.18309	−68.7548	−12.6236	−28.2462	−47.669
91715794	TbAT1	−55.8875	−8.55159	−70.2583	−3.75554	−29.4483	−54.2456
14440539	TbAT1	−40.6711	−8.60008	−74.2061	−7.99181	−30.1235	−55.8887
6442560	TbAT1	−48.1948	−8.40646	−69.8895	−4.43734	−30.5629	−53.9663
550286	TbAT1	−31.5112	−8.07276	−40.3092	−6.76122	−16.4097	−28.2781
71357126	TbAT1	−44.6042	−8.06138	−57.6981	−9.66823	−23.8084	−39.9465
71357126	Casein kinase	−39.9705	−8.06672	−68.2929	−11.1469	−27.7441	−45.1234
31211	Leucyl tRNA synthetase	−41.0339	−8.08338	−50.9063	−12.5422	−15.9189	−30.3871
6442560	MRP E	−46.2196	−8.08799	−79.0799	−15.4979	−28.3857	−53.0275

The XP docking revealed significant hydrogen bonds (H-bonds) and Pi-Pi stacking of phytochemicals for MZ. [6]-Isoshogaol formed H-bonds at TYR 31 and ASN 407 with TbAT1, having bond lengths of 2.42 and 1.83 Å, respectively. Regarding the same protein, [10]-Gingerol monoacetate formed three H-bonds at ASN 346 (1.94 Å), ARG 353 (2.52 Å), and ASN 407 (2.12 Å). [6]-Gingerdione also formed two H-bonds involving TYR 31 (1.89 Å) and ASN 66 (1.78 Å). However, 8-Shogaol interacted through a Pi-Pi stacking with TYR 31 (4.19 Å) and an H-bond with ASN 346 (1.85 Å) in the active binding pocket of TbAT1. Moreover, 1-(4-Hydroxy-3-methoxyphenyl)oct-4-en-3-one formed H-bonds with ASN 28 (1.75 Å), ASN 407 (1.97 Å), and a Pi-Pi stacking with PHE 345 (5.42 Å) (Supplementary Table S1).

Additionally, 1-(4-Hydroxy-3-methoxyphenyl)oct-4-en-3-one interacted with casein kinase through a single H-bond at ASP 366 (1.79 Å). Zingerone formed four interactions, including three H-bonds with leucyl-tRNA synthetase at ILE 228, ARG 242 (1.94 Å), and ALA 569 (2.04 Å), and one Pi-Pi stacking at TRP 571 (5.38 Å). Lastly, MRP E also showed interaction through H-bond with ASN 1362 (1.78 Å) (Supplementary Figure S1).

3.9. ADMET Analysis

The ADMET prediction of the phytocompounds identified from molecular docking studies revealed significantly favorable drug-like properties. [6]-Isoshogaol and 8-Shogaol had comparatively higher lipophilicity (QPlog Po/w; 3.988 and 4.811, respectively). On the other hand, zingerone and 2,3,4,6-tetrahydro-1,6-benzoxazocin-5-one showed comparatively lower lipophilicity. [6]-Isoshogaol had the highest dipole moment (5.713) and surface accessible surface area (SASA; 632.75). Additionally, [6]-Gingerol monoacetate (128.327) and [10]-Gingerdione (128.449) also had the highest polar surface areas (Frac-

tional Ionization Surface Area). All other compounds, except for zingerone (90.53%) and 2,3,4,6-tetrahydro-1,6-benzoxazocin-5-one (94.823%), showed 100% human oral absorption. Moreover, 8-Shogaol revealed a high QPlogHERG value (−5.823), which is suggestive of potential cardiotoxicity. Furthermore, 2,3,4,6-Tetrahydro-1,6-benzoxazocin-5-one revealed the highest brain penetration potential (QPlogBB; 0.024). [6]-Isoshogaol appeared to be the best candidate for further evaluation based on its balanced ADMET properties (Supplementary Table S2).

3.10. Molecular Dynamics Simulation

The MD simulation results of the TbAT1 complexed with 6-Isoshogaol, analyzed over a 50 ns trajectory, revealed a relatively stable binding conformation (root mean square deviation) with slight fluctuations of around 1.0 Å. Minor variations of around 5.0 Å were recorded regarding the radius of gyration. The molecular surface area also fluctuated slightly by 320 Å^2. In contrast, a sharp decline at approximately 5 ns and later stabilization at approximately 30 Å^2 were observed for the solvent-accessible surface area. The polar surface area (PSA) remained relatively stable around 100 Å^2 and reflected the consistent interactions between polar groups and the solvent environment (Figure 5).

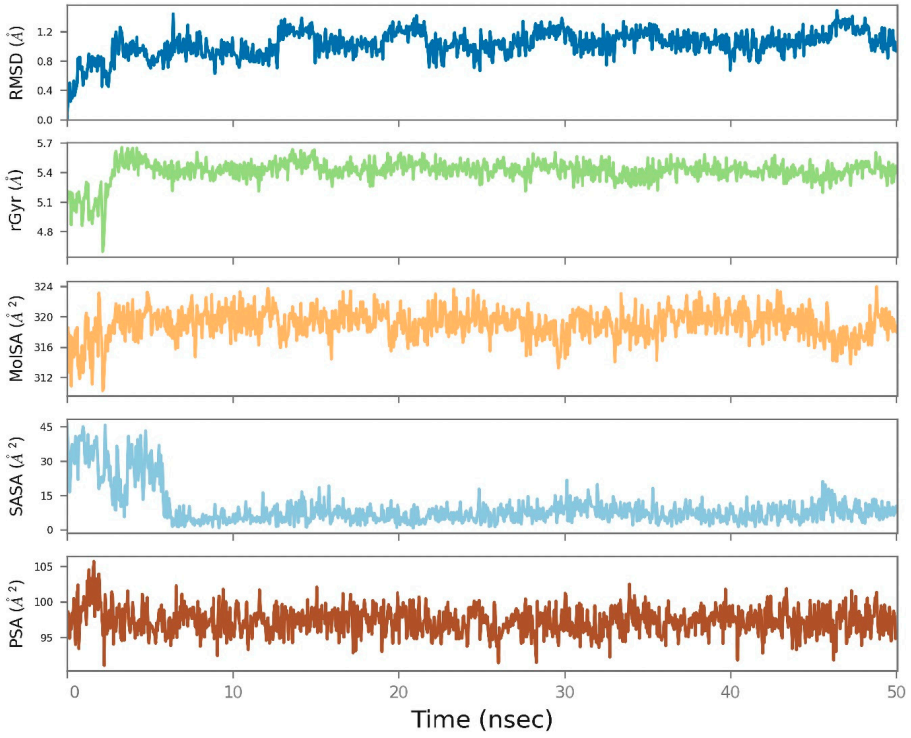

Figure 5. Molecular dynamics simulation results of the TbAT1 complexed with 6-Isoshogaol over a 50 ns trajectory. The root mean square deviation (RMSD), radius of gyration (rGyr), molecular surface area (MoISA), solvent-accessible surface area (SASA), and polar surface area (PSA) plots show the structural stability, compactness, and consistent surface exposure throughout the simulation.

4. Discussion

Trypanosomiasis remains a significant health concern in humans and animals, characterized by a complex interplay between host responses and parasite activities, resulting in biochemical, histological, and physiological alterations during infection. In the present study, phytochemical screening of MZ revealed the presence of sesquiterpenes, phenolic compounds, and capsaicinoids. Several investigators have discovered tannins, phenolics, alkaloids, and flavonoids in plants exhibiting trypanicidal properties [44,45]. They hypothesized that the trypanicidal properties of the extract may result from the activity of

one or more compounds found in the plant [46,47]. However, the mechanism behind the trypanicidal activity was not elucidated. Computer-aided drug discovery has been essential in reinforcing the conventional methods in terms of time and cost [48]. To our knowledge, this study is the first to propose the possible mechanism of action of phytoconstituents of *MZ* through computational methods targeting various essential proteins of *T. evansi*.

Earlier investigations have shown that natural products contain components that may generate radicals, potentially leading to peroxidative damage to enzymes, which are highly sensitive to changes in the redox equilibrium [49]. Some drugs have also been observed to bind with the kinetoplast DNA of trypanosomes [50]. Sepúlveda-Boza and Cassels [51] indicated that some natural compounds display trypanicidal activity by disrupting the redox equilibrium of the parasites, either by targeting the respiratory chain or by compromising the parasite's cell defense against oxidative stress.

The administration of *MZ* resulted in reduced parasitemia levels in the experimentally infected mice. It also improved body weights and survival time in the mice in a dose-dependent manner. The trypanicidal activity recorded in the present study may be attributed to the combined effect of MZ phytoconstituents. In our study, the bioactive phenolic compounds of MZ, including 6-Isoshogaol, 6-Gingerol monoacetate, 10-gingerdione, 8-Shogaol, 1-(4-hydroxy-3-methoxyphenyl)oct-4-en-3-one, 2,3,4,6-tetrahydro-1,6-benzoxazocin-5-one, and zingerone, have been predicted to exhibit significant interactions with several essential proteins of *T. evansi*. 6-Isoshogaol is a dehydrated derivative of gingerol [52] and has previously exhibited potent anti-inflammatory properties, primarily through the inhibition of nuclear factor kappa B (NF-κB) signaling [53]. Studies have reported favorable pharmacokinetics, characterized by rapid hepatic metabolism and enhanced bioavailability [54]. 6-Gingerol monoacetate is a more stable analog [55] and has shown promising anticancer activity [56]. 10-Gingerdione has been reported to have antioxidant and anti-inflammatory effects, though its pharmacokinetics are less explored [57]. 8-Shogaol is a thermally stable constituent of *Z. officinale* and is quickly absorbed and metabolized through conjugation reactions [58]. The phenolic compound 1-(4-Hydroxy-3-methoxyphenyl)oct-4-en-3-one has been previously reported to have antioxidant and antidiabetic activities. However, the reduced trypanocidal efficacy of crude MZ compared with isometamidium chloride could also be due to enzymatic inactivation of active compounds, impaired absorption from the gut, or both [59,60]. Additionally, the efficacy of extracts may also require administration via parenteral route [61].

Additionally, the improvement in hematobiochemical parameters was also observed in the MZ-treated groups in a dose-dependent manner. At higher doses, the results were comparable to those of the treated control group. Various researchers have reported that the pathological effects in trypanosomiasis are initiated through the release of cytokines and nitric oxide [62,63]. Polyphenols have demonstrated the capacity to mitigate cytokine- and nitric oxide-induced inflammation, possibly due to their ability to scavenge reactive oxygen species (ROS) [64].

The immune system plays a vital part in defending the body, aiding in recovery from illness, and lowering the risk of both infectious and long-term diseases [65]. Strengthening immunity can be achieved by consuming a well-balanced diet enriched with essential nutrients, including vitamins, minerals, and biologically active compounds [65]. However, in conditions such as trypanosomiasis, the body may produce excessive ROS, which overwhelm the natural antioxidant defenses [66]. In such cases, the body requires additional antioxidants obtained from daily dietary sources. These externally sourced antioxidants, known as exogenous antioxidants, include compounds like ascorbic acid or vitamin C, which neutralize hydroxyl and superoxide radicals; tocopherols or vitamin E, which help prevent the oxidation of cell membrane lipids; and a range of phenolic compounds, such

as flavonoids, resveratrol, and phenolic acids [67]. Other supportive nutrients include oil-based lecithin, as well as minerals like selenium and zinc [68]. When the intake of these antioxidants is insufficient, it can lead to an imbalance between free radical generation and antioxidant availability, resulting in a condition known as oxidative stress [69].

The elevated MDA levels in the brain tissue detected in the present study suggest the ability of *T. evansi* to induce lipid peroxidation due to ROS. These findings are in agreement with previous studies that have shown trypanosomiasis induces lipid peroxidation in infected cattle [70,71]. Notably, significantly decreased concentrations of oxidative stress markers (i.e., MDA) and elevated antioxidant defense markers such as CAT and SOD, corresponding with lower genotoxicity scores in brain tissues of infected mice after treatment with MZ in a dose-dependent manner. These variations can be explained by the host–parasite interaction, where *T. evansi* induces excessive ROS generation that overwhelms endogenous antioxidant defenses, leading to oxidative stress and genotoxicity in neuronal tissues [72]. Similar mechanisms of parasite-induced oxidative imbalance have been reported in trypanosome-infected models, with alterations in CAT and SOD activities directly linked to disease severity [73]. The observed restoration of antioxidant enzyme activity and reduction in DNA damage following MZ treatment suggest that ginger-derived compounds may stabilize redox homeostasis and confer neuroprotection during infection [74].

Z. officinale exhibits strong antioxidant activity due to the presence of biologically active compounds such as shogaol, gingerol, zingerone, and paradol, which contribute to the reduction of ROS [75]. *Z. officinale* promotes the restoration of antioxidant enzymes like catalase and superoxide dismutase, increases glutathione levels, inhibits lipid peroxidation, reduces nitric oxide (NO) production, and neutralizes hydroxyl radicals [76]. It also significantly downregulates the gene expression of inducible nitric oxide synthase (iNOS), decreases caspase-3 positive cells, and lowers tumor necrosis factor alpha (TNF-α) expression, collectively reducing ROS formation and disrupting MAPK-related signaling pathways [77]. In addition, the bioactive compounds present in *Z. officinale* have the ability to increase the expression of key antioxidant proteins such as glutathione, heme oxygenase-1, quinone oxidoreductase-1, metallothionein 1, aldo-keto reductase family 1 member B10 (AKR1B10), ferritin light chain, and gamma-glutamyltransferase-like activity 4 through Nrf2 signaling pathway activation [78–80]. These compounds also suppress the synthesis of the pro-apoptotic protein (Bax) and prevent the production of oxidative stress mediators such as hydrogen peroxide, malondialdehyde, and myeloperoxidase [81]. Furthermore, *Z. officinale* activates protein kinase B and phosphatidylinositol-3-kinase (PI3K) in activated B cells, offering cellular protection against oxidative and inflammatory damage [75]. This regulation of gene expression supports the increased production of antioxidant enzymes like SOD, catalase, and glutathione peroxidase, as well as the synthesis of glutathione [76]. As a result, it helps reduce the formation of reactive oxygen and nitrogen species, lowers levels of lipid peroxidation products such as malondialdehyde and myeloperoxidase, and ultimately mitigates oxidative stress, DNA damage, and cell death [64]. These mechanistic pathways help explain our findings, which show that MZ reduced MDA levels, restored CAT and SOD activity, and lowered DNA damage in infected brain tissue. The in silico results further support this by highlighting [6]-Isoshogaol and [6]-Gingerol as lead compounds with stable interactions against key *T. evansi* proteins, reinforcing their role in alleviating oxidative stress and genotoxicity.

In this study, the key proteins such as TbAT1, casein kinase, leucyl-tRNA synthetase, and MRP E with critical roles in parasite survival and pathogenicity have been predicted as promising targets of phytochemicals from MZ. TbAT1 is involved in the uptake of purines that trypanosomes cannot synthesize de novo, which makes it essential for parasite

proliferation [82]. Furthermore, resistance against drugs has been associated with mutations in TbAT1, indicating it as a possible target for mitigating drug resistance [83]. Moreover, casein kinase is a serine/threonine protein kinase involved in the control of the cell cycle and signaling pathways. It also maintains the energy homeostasis [84]. Inhibiting the protein kinases disrupts parasite replication and also offers a pathway for therapeutic intervention. Aminoacyl-tRNA synthetases (aaRSs) are necessary for accurately pairing free amino acids with their corresponding tRNA. Their role in protein synthesis makes them a compelling target for antimicrobial therapies [85,86]. aaRSs synthetases represent a promising target for the identification of broad-spectrum anti-trypanosomal agents, with minimal impact on the human equivalent target [87]. Leucyl-tRNA synthetase is essential for catalyzing the attachment of leucine to its corresponding tRNA [88]. Its inhibition could possibly halt protein production, resulting in the death of the parasite [89]. Lastly, there is a scarcity of data regarding the MRP E gene in *T. evansi* [90,91]. MRP E is a member of the ATP-binding cassette transporter family and is essential for certain resistance of *Trypanosoma* species to trypanocides [92,93]. Inhibition of MRP E can enhance the efficacy of current trypanocidal drugs by preventing drug elimination from the parasite [94].

The ADMET study yielded significant insights into the pharmacokinetic and physicochemical features of seven ginger-derived bioactive compounds, with 6-Isoshogaol exhibiting a superior profile as a trypanicidal candidate. 6-Isoshogaol exhibited a balanced lipophilicity (QPlog Po/w = 3.988), indicative of optimal permeability through biological membranes, in contrast to the comparatively elevated lipophilicity of 8-Shogaol (QPlog Po/w = 4.811). Furthermore, the largest dipole moment (5.713) was recorded for 6-Isoshogaol. The findings suggest better interaction with polar environments. Conversely, zingerone and 2,3,4,6-tetrahydro-1,6-benzoxazocin-5-one demonstrated reduced lipophilicity values (QPlog Po/w = 1.758 and 1.431, respectively), perhaps constraining their membrane permeability and absorption efficacy. In contrast to zingerone (90.53%) and 2,3,4,6-tetrahydro-1,6-benzoxazocin-5-one (94.823%), 6-Isoshogaol exhibited complete human oral absorption. Significantly, its adherence to both the Rule of Five and the Rule of Three demonstrated its advantageous drug-likeness. The cardiotoxicity potential (QPlogHERG values) was more favorable for 6-Isoshogaol (−5.293) compared with the increased risk associated with 8-Shogaol (−5.823).

Results of ADMET analysis and MD simulation revealed 6-Isoshogaol with balanced pharmacokinetic properties and stable binding conformation, predicting it as a potential candidate for in vitro and in vivo evaluation.

5. Conclusions

Zingiber officinale extract showed strong trypanocidal, antioxidant, and neuroprotective effects against *T. evansi*. [6]-Isoshogaol and [6]-Gingerol emerged as lead compounds, supporting ginger-derived molecules as promising candidates for natural trypanocidal therapy.

Supplementary Materials: The following supporting information can be downloaded at: https://www.mdpi.com/article/10.3390/oxygen5030019/s1, Figure S1: Graphical representation of molecular interactions between various compounds and their protein targets; Table S1: Ligand interactions with protein targets including TbAT1, casein kinase, leucyl-tRNA synthetase, and multi-drug resistance protein E; Table S2: Key physicochemical and pharmacokinetic properties of seven ginger-derived compounds ([6]-Isoshogaol, [6]-Gingerol monoacetate, [10]-Gingerdione, 8-Shogaol, 1-(4-Hydroxy-3-methoxyphenyl)oct-4-en-3-one, 2,3,4,6-tetrahydro-1,6-benzoxazocin-5-one, and zingerone).

Author Contributions: Conceptualization, W.A., M.Y.T., and H.A.; methodology, W.A. and H.A.; software, W.A.; validation, M.u.R.K.; formal analysis, W.A. and A.A.A.; investigation, W.A., H.A., and M.O.O.; resources, H.A.; data curation, W.A.; writing—original draft preparation, W.A. and M.Y.T.; writing—review and editing, M.Y.T.; visualization, W.A.; supervision, M.Y.T. All authors have read and agreed to the published version of the manuscript.

Funding: This research received no external funding.

Institutional Review Board Statement: The study was conducted in accordance with the Declaration of Helsinki for animals and approved by the Institutional Ethical Review Committee of University of Veterinary and Animal Sciences, Lahore, Pakistan (No. DR. 430. Dated 26 September 2023).

Informed Consent Statement: Not applicable.

Data Availability Statement: All the data is available in the manuscript.

Conflicts of Interest: The authors declare no conflicts of interest.

Abbreviations

The following abbreviations are used in this manuscript:

MZ	Methanolic extract of *Zingiber officinale*
T. evansi	*Trypanosoma evansi*
TC	Treated Control
UC	Untreated Control
GC-MS	Gas Chromatography–Mass Spectrometry
HPLC	High-Performance Liquid Chromatography
PSG	Phosphate Saline Glucose
DPI	Days Post-Infection
CAT	Catalase
MDA	Malondialdehyde
SOD	Superoxide Dismutase
ALT	Alanine Transaminase
AST	Aspartate Transaminase
Hb	Hemoglobin
RBC	Red Blood Cells
TLC	Total Leukocyte Count
Hct	Hematocrit
MCV	Mean Corpuscular Volume
MCH	Mean Corpuscular Hemoglobin
MCHC	Mean Corpuscular Hemoglobin Concentration
A/G Ratio	Albumin/Globulin Ratio
GDI	Genetic Damage Index
MD	Molecular Dynamics
XP	Extra Precision (Docking Mode)
vdW	Van der Waals
ADMET	Absorption, Distribution, Metabolism, Excretion, and Toxicity
QPlog Po/w	Octanol/Water Partition Coefficient (LogP)
QPlog S	Predicted Aqueous Solubility
QPlog HERG	Predicted HERG Channel Blockage
QPlog BB	Predicted Blood-Brain Barrier Permeability
QPlog Kp	Predicted Skin Permeability
SASA	Solvent Accessible Surface Area
FISA	Hydrophilic Interaction Surface Area
PSA	Polar Surface Area
SWISS-MODEL	Swiss Automated Homology Modeling Server
RMSD	Root Mean Square Deviation

PI3K	Phosphatidylinositol-3-Kinase
NF-κB	Nuclear Factor kappa-light-chain-enhancer of activated B cells
TNF-α	Tumor Necrosis Factor Alpha
iNOS	Inducible Nitric Oxide Synthase
AKR1B10	Aldo-Keto Reductase Family 1 Member B10
MRP E	Multidrug Resistance Protein E
TbAT1	*Trypanosoma brucei* Adenosine Transporter 1

References

1. Baker, R.E.; Mahmud, A.S.; Miller, I.F.; Rajeev, M.; Rasambainarivo, F.; Rice, B.L.; Takahashi, S.; Tatem, A.J.; Wagner, C.E.; Wang, L.-F. Infectious disease in an era of global change. *Nat. Rev. Microbiol.* **2022**, *20*, 193–205. [CrossRef]
2. Iqbal, M.S.; Akbar, H.; Sarfraz-ur-Rahman, S.I.; Nabi, H.; Hussain, N.; MI, R. Optimization of "loop mediated isothermal amplification" lamp technique for the molecular diagnosis of surra in domestic animals. *Vet. Sci. One Health J.* **2022**, *1*, 1–15.
3. Aregawi, W.G.; Agga, G.E.; Abdi, R.D.; Büscher, P. Systematic review and meta-analysis on the global distribution, host range, and prevalence of *Trypanosoma evansi*. *Parasites Vectors* **2019**, *12*, 1–25. [CrossRef]
4. Sengupta, P.P.; Jacob, S.S.; Chandu, A.G.S.; Das, S. Silent *Trypanosoma evansi* infection in humans from India revealed by serological and molecular surveys, and characterized by variable surface glycoprotein gene sequences. *Acta Trop.* **2022**, *229*, 106369. [CrossRef]
5. Jain, P.; Goyal, V.; Agrawal, R. An atypical Trypanosoma lewisi infection in a 22-day-old neonate from India: An emergent zoonosis. *Indian. J. Pathol. Microbiol.* **2023**, *66*, 199–201. [CrossRef]
6. Diall, O.; Desquesnes, M.; Faye, B.; Dia, M.L.; Jacquiet, P.; Sazmand, A.; Otranto, D.; Touratier, L. Development of a control strategy towards elimination of *Trypanosoma evansi* infection (surra) in camels in Africa. *Acta Trop.* **2022**, *234*, 106583. [CrossRef]
7. Kasozi, K.I.; MacLeod, E.T.; Ntulume, I.; Welburn, S.C. An update on African trypanocide pharmaceutics and resistance. *Front. Vet. Sci.* **2022**, *9*, 828111. [CrossRef]
8. Mdachi, R.E.; Ogolla, K.O.; Auma, J.E.; Wamwiri, F.N.; Kurgat, R.K.; Wanjala, K.B.; Mugunieri, L.G.; Alusi, P.M.; Chemuliti, J.K.; Mukiria, P.W. Variation of sensitivity of *Trypanosoma evansi* isolates from Isiolo and Marsabit counties of Kenya to locally available trypanocidal drugs. *PLoS ONE* **2023**, *18*, e0281180. [CrossRef] [PubMed]
9. Kayser, O.; Masihi, K.N.; Kiderlen, A.F. Natural products and synthetic compounds as immunomodulators. *Expert. Rev. Anti-Infect. Ther.* **2003**, *1*, 319–335. [CrossRef] [PubMed]
10. Newman, D.J.; Cragg, G.M. Natural products as sources of new drugs from 1981 to 2014. *J. Nat. Prod.* **2016**, *79*, 629–661. [CrossRef]
11. Nandi, S.; Rahman, M.Z.; Siraj, S.; Ahmed, S.; Ahsan, M.A.; Sultana, N.; Bhuiyan, M.N.H.; Rahim, M.M.; Saleh-e-In, M.M.; Roy, S.K. Quality composition and biological significance of the Bangladeshi and China ginger (*Zingiber officinale* Rosc.). *J. Microbiol. Biotechnol. Food Sci.* **2013**, *2*, 2283–2290.
12. Mahboubi, M. *Zingiber officinale* Rosc. essential oil, a review on its composition and bioactivity. *Clin. Phytoscience* **2019**, *5*, 1–12. [CrossRef]
13. Sanderson, L.; Bartlett, A.; Whitfield, P. In vitro and in vivo studies on the bioactivity of a ginger (*Zingiber officinale*) extract towards adult schistosomes and their egg production. *J. Helminthol.* **2002**, *76*, 241–247. [CrossRef]
14. Moazeni, M.; Nazer, A. In vitro lethal effect of *Zingiber officinale* R. on protoscolices of hydatid cyst from sheep liver. *Microbiol. Res.* **2011**, *2*, e25. [CrossRef]
15. Merawin, L.; Arifah, A.; Sani, R.; Somchit, M.; Zuraini, A.; Ganabadi, S.; Zakaria, Z. Screening of microfilaricidal effects of plant extracts against *Dirofilaria immitis*. *Res. Vet. Sci.* **2010**, *88*, 142–147. [CrossRef]
16. El-Melegy, M.; El-Saify, G.; Hassab-El-Nabi, S. Evaluation of therapeutic effect of ginger compared to flubendazole on experimental trichinelosis in mice. *Egyp J. Med. Sci.* **2006**, *27*, 25–48.
17. Montazeri, M.; Sharif, M.; Sarvi, S.; Mehrzadi, S.; Ahmadpour, E.; Daryani, A. A systematic review of in vitro and in vivo activities of anti-Toxoplasma drugs and compounds (2006–2016). *Front. Microbiol.* **2017**, *8*, 228484. [CrossRef] [PubMed]
18. Kobo, P.; Erin, P.; Suleiman, M.; Aliyu, H.; Tauheed, M.; Muftau, S.; Mamman, M. Antitrypanosomal effect of methanolic extract of *Zingiber officinale* (ginger) on *Trypanosoma brucei brucei*-infected Wistar mice. *Vet. World* **2014**, *7*, 770–775. [CrossRef]
19. Padhy, I.; Mahapatra, A.; Banerjee, B.; Sharma, T. Computational approaches in drug discovery from phytochemicals. In *Phytochemistry, Computational Tools and Databases in Drug Discovery*; Elsevier: Amsterdam, The Netherlands, 2023; pp. 57–88.
20. Sharif, M.F.; Bennett, M.T. The effect of different methods and solvents on the extraction of polyphenols in ginger (*Zingiber officinale*). *J. Teknol.* **2016**, *78*, 49–54. [CrossRef]
21. El-Kady, A.M.; Al-Megrin, W.A.I.; Abdel-Rahman, I.A.; Sayed, E.; Alshehri, E.A.; Wakid, M.H.; Baakdah, F.M.; Mohamed, K.; Elshazly, H.; Alobaid, H.M. Ginger is a potential therapeutic for chronic toxoplasmosis. *Pathogens* **2022**, *11*, 798. [CrossRef]

22. Khan, S.; Arshad, S.; Masood, I.; Arif, A.; Abbas, S.; Qureshi, A.W.; Parveen, A.; Seemab Ameen, Z. GC–MS Analysis of *Persicaria bistorta*: Uncovering the Molecular Basis of Its Traditional Medicinal Use. *Appl. Biochem. Biotechnol.* **2024**, *196*, 2270–2288. [CrossRef] [PubMed]
23. Ahmad, W.; Tipu, M.Y.; Khan, M.u.R.; Akbar, H.; Anjum, A.A.; Omer, M.O. Molecular characterization, oxidative stress-mediated genotoxicity, and hemato-biochemical changes in domestic water buffaloes naturally infected with *Trypanosoma evansi* under field conditions. *Pathogens* **2025**, *14*, 66. [CrossRef]
24. Baldissera, M.D.; Souza, C.F.; Riéffel, R.C.; Velho, M.C.; Ramos, A.P.; Nascimento, K.; Sagrillo, M.R.; Ourique, A.F.; da Silva, A.S.; Stefani, L.M. Protective effect of nerolidol-loaded in nanospheres against cerebral damage caused by *Trypanosoma evansi*. *N-S Arch. Pharmacol.* **2018**, *391*, 753–759. [CrossRef]
25. Herbert, W.; Lumsden, W. *Trypanosoma brucei*: A rapid "matching" method for estimating the host's parasitemia. *Exp. Parasitol.* **1976**, *40*, 427–431. [CrossRef]
26. Committee for the Update of the Guide for the Care and Use of Labotayory Animals; Institute for Laboratory Animals Research; Division on Earth and Life Studies; National Research Council. *Guide for the Care and Use of Laboratory Animals*, 8th ed.; The National Academies Press: Washington, DC, USA, 2010.
27. Singh, T.B.; Mukhopadhayay, S.K.; Sar, T.K.; Ganguly, S. Acetamiprid induces toxicity in mice under experimental conditions with prominent effect on the hematobiochemical parameters. *J. Drug Metab. Toxicol.* **2012**, *3*, 134. [CrossRef]
28. Monzem, S.; Gohin, S.; Yagüe Ballester, R.; Lopes de Souza, R.; Meeson, R.; Pitsillides, A.A. An examination of two different approaches for the study of femoral neck fracture: Towards a more relevant rodent model. *Proc. Inst. Mech. Eng. Part. H J. Eng. Med.* **2022**, *236*, 199–207. [CrossRef]
29. Nishikimi, M.; Rao, N.A.; Yagi, K. The occurrence of superoxide anion in the reaction of reduced phenazine methosulfate and molecular oxygen. *Biochem. Biophys. Res. Commu.* **1972**, *46*, 849–854. [CrossRef]
30. Bakar, E.; Ulucam, E.; Cerkezkayabekir, A. Protective effects of proanthocyanidin and vitamin E against toxic effects of formaldehyde in kidney tissue. *Biotec. Histochem.* **2015**, *90*, 69–78. [CrossRef] [PubMed]
31. Ranjith, H.V.; Sagar, D.; Kalia, V.K.; Dahuja, A.; Subramanian, S. Differential Activities of Antioxidant Enzymes, Superoxide Dismutase, Peroxidase, and Catalase vis-à-vis Phosphine Resistance in Field Populations of Lesser Grain Borer (*Rhyzopertha dominica*) from India. *Antioxidants.* **2023**, *12*, 270. [CrossRef]
32. Beers, R.F.; Sizer, I.W. A spectrophotometric method for measuring the breakdown of hydrogen peroxide by catalase. *J. Biol. Chem.* **1952**, *195*, 133–140. [CrossRef]
33. Tice, R.R.; Agurell, E.; Anderson, D.; Burlinson, B.; Hartmann, A.; Kobayashi, H.; Miyamae, Y.; Rojas, E.; Ryu, J.C.; Sasaki, Y. Single cell gel/comet assay: Guidelines for in vitro and in vivo genetic toxicology testing. *Environ. Mol. Mutagen.* **2000**, *35*, 206–221. [CrossRef]
34. Ahmad, W.; Sattar, A.; Ahmad, M.; Aziz, M.W.; Iqbal, A.; Tipu, M.Y.; Mushtaq, R.M.Z.; Rasool, N.; Ahmed, H.S.; Ahmad, M. Unveiling Oxidative Stress-Induced Genotoxicity and Its Alleviation through Selenium and Vitamin E Therapy in Naturally Infected Cattle with Lumpy Skin Disease. *Vet. Sci.* **2023**, *10*, 643. [CrossRef]
35. Ramachandran, G. Molecular structure of collagen. *Int. Rev. Connect. Tissue Res.* **1963**, *1*, 127–182.
36. Dym, O.; Eisenberg, D.; Yeates, T. ERRAT. *Int. Tables Crystallogr.* **2012**, *21*, 678–679.
37. Garg, V.K.; Avashthi, H.; Tiwari, A.; Jain, P.A.; Ramkete, P.W.; Kayastha, A.M.; Singh, V.K. MFPPI–multi FASTA ProtParam interface. *Bioinformation* **2016**, *12*, 74. [CrossRef] [PubMed]
38. Hatami, S.; Sirous, H.; Mahnam, K.; Najafipour, A.; Fassihi, A. Preparing a database of corrected protein structures important in cell signaling pathways. *Res. Pharm. Sci.* **2023**, *18*, 67–78. [CrossRef] [PubMed]
39. Suri, C.; Joshi, H.C.; Naik, P.K. Molecular modeling reveals binding interface of γ-tubulin with GCP4 and interactions with noscapinoids. *Proteins: Struct. Funct. Bioinform.* **2015**, *83*, 827–843. [CrossRef]
40. Dolghih, E.; Bryant, C.; Renslo, A.R.; Jacobson, M.P. Predicting binding to p-glycoprotein by flexible receptor docking. *PLoS Comput. Biol.* **2011**, *7*, e1002083. [CrossRef]
41. Singh, A.K.; Bilal, M.; Iqbal, H.M.; Raj, A. In silico analytical toolset for predictive degradation and toxicity of hazardous pollutants in water sources. *Chemosphere* **2022**, *292*, 133250. [CrossRef] [PubMed]
42. Du, J.; Sun, H.; Xi, L.; Li, J.; Yang, Y.; Liu, H.; Yao, X. Molecular modeling study of checkpoint kinase 1 inhibitors by multiple docking strategies and prime/MM–GBSA calculation. *J. Comput. Chem.* **2011**, *32*, 2800–2809. [CrossRef]
43. Ioakimidis, L.; Thoukydidis, L.; Mirza, A.; Naeem, S.; Reynisson, J. Benchmarking the reliability of QikProp. Correlation between experimental and predicted values. *QSAR Comb. Sci.* **2008**, *27*, 445–456. [CrossRef]
44. Setzer, W.N.; Ogungbe, I.V. In-silico investigation of antitrypanosomal phytochemicals from Nigerian medicinal plants. *PLoS Neglected Trop. Dis.* **2012**, *6*, e1727. [CrossRef]
45. Mergia, E.; Shibeshi, W.; Terefe, G.; Teklehaymanot, T. Antitrypanosomal activity of Verbascum sinaiticum Benth.(Scrophulariaceae) against Trypanosoma congolense isolates. *BMC Complement. Altern. Med.* **2016**, *16*, 1–9. [CrossRef] [PubMed]

46. Ogbadoyi, E.O.; Abdulganiy, A.O.; Adama, T.Z.; Okogun, J.I. In vivo trypanocidal activity of *Annona senegalensis* Pers. leaf extract against *Trypanosoma brucei brucei*. *J. Ethnopharmacol.* **2007**, *112*, 85–89. [CrossRef]
47. Morais, M.C.d.; Souza, J.V.d.; da Silva Maia Bezerra Filho, C.; Dolabella, S.S.; Sousa, D.P.d. Trypanocidal essential oils: A review. *Molecules* **2020**, *25*, 4568. [CrossRef]
48. Makhouri, F.R.; Ghasemi, J.B. Combating diseases with computational strategies used for drug design and discovery. *Curr. Top. Med. Chem.* **2018**, *18*, 2743–2773. [CrossRef]
49. Lopes Pereira, P.M.; Carreira de Paula, J. Antiprotozoal Activity of Benzoylthiourea Derivatives against Trypanosoma cruzi: Insights into Mechanism of Action. *Pathogens* **2023**, *2*, 1012. [CrossRef]
50. Sodhi, K.K.; Shree, P.; Mishra, L.C.; Mishra, G.; Kumar, M.; Singh, D.K. Promising Compounds of Plant Origin and Their Synthetic Analogs Against Trypanosomes. In *Natural Product Based Drug Discovery Against Human Parasites: Opportunities and Challenges*; Springer: Berlin/Heidelberg, Germany, 2023; pp. 411–429.
51. Sepúlveda-Boza, S.; Cassels, B.K. Plant metabolites active against Trypanosoma cruzi. *Planta Médica* **1996**, *62*, 98–105. [CrossRef] [PubMed]
52. Jolad, S.D.; Lantz, R.C.; Chen, G.J.; Bates, R.B.; Timmermann, B.N. Commercially processed dry ginger (*Zingiber officinale*): Composition and effects on LPS-stimulated PGE2 production. *Phytochemistry* **2005**, *66*, 1614–1635. [CrossRef]
53. Nigam, N.; George, J.; Shukla, Y. Ginger (6-gingerol). In *Molecular Targets and Therapeutic Uses of Spices: Modern Uses for Ancient Medicine*; World Scientific: New Jersey, NJ, USA, 2009; pp. 225–256.
54. Kubra, I.R.; Rao, L.J.M. An impression on current developments in the technology, chemistry, and biological activities of ginger (*Zingiber officinale Roscoe*). *Crit. Rev. Food Sci. Nutr.* **2012**, *52*, 651–688. [CrossRef]
55. Stan, D.; Enciu, A.-M.; Mateescu, A.L.; Ion, A.C.; Brezeanu, A.C.; Stan, D.; Tanase, C. Natural compounds with antimicrobial and antiviral effect and nanocarriers used for their transportation. *Front. Pharmacol.* **2021**, *12*, 723233. [CrossRef]
56. Sp, N.; Kang, D.Y.; Lee, J.-M.; Bae, S.W.; Jang, K.-J. Potential antitumor effects of 6-gingerol in p53-dependent mitochondrial apoptosis and inhibition of tumor sphere formation in breast cancer cells. *Int. J. Mol. Sci.* **2021**, *22*, 4660. [CrossRef]
57. Yücel, Ç.; Karatoprak, G.Ş.; Açıkara, Ö.B.; Akkol, E.K.; Barak, T.H.; Sobarzo-Sánchez, E.; Aschner, M.; Shirooie, S. Immunomodulatory and anti-inflammatory therapeutic potential of gingerols and their nanoformulations. *Front. Pharmacol.* **2022**, *13*, 902551. [CrossRef]
58. Geng, J.; Chen, C.; Pan, D.; Wang, Q. Exploring the therapeutic effects of Zingiberis Rhizoma Preparatum (Pao-Jiang) against DSS-induced ulcerative colitis in mice by metabolomics-guided analysis. *J. Holist. Integr. Pharm.* **2023**, *4*, 272–280. [CrossRef]
59. Al-Ishaq, R.K.; Liskova, A.; Kubatka, P.; Büsselberg, D. Enzymatic metabolism of flavonoids by gut microbiota and its impact on gastrointestinal cancer. *Cancers* **2021**, *13*, 3934. [CrossRef]
60. Braune, A.; Engst, W.; Elsinghorst, P.W.; Furtmann, N.; Bajorath, J.; Gütschow, M.; Blaut, M. Chalcone isomerase from Eubacterium ramulus catalyzes the ring contraction of flavanonols. *J. Bacteriol.* **2016**, *198*, 2965–2974. [CrossRef]
61. Zolkepli, H.; Widodo, R.T.; Mahmood, S.; Salim, N.; Awang, K.; Ahmad, N.; Othman, R. A review on the delivery of plant-based antidiabetic agents using nanocarriers: Current status and their role in combatting hyperglycaemia. *Polymers* **2022**, *14*, 2991. [CrossRef]
62. Pays, E.; Radwanska, M.; Magez, S. The pathogenesis of African trypanosomiasis. *Annu. Rev. Pathol.* **2023**, *18*, 19–45. [CrossRef] [PubMed]
63. Macaluso, G.; Grippi, F.; Di Bella, S.; Blanda, V.; Gucciardi, F.; Torina, A.; Guercio, A.; Cannella, V. A Review on the Immunological Response against *Trypanosoma cruzi*. *Pathogens* **2023**, *12*, 282. [CrossRef] [PubMed]
64. Subedi, L.; Gaire, B.P.; Kim, S.-Y.; Parveen, A. Nitric oxide as a target for phytochemicals in anti-neuroinflammatory prevention therapy. *Int. J. Mol. Sci.* **2021**, *22*, 4771. [CrossRef] [PubMed]
65. Cumming, E.; Peters, C. Immune response to infection. *Anaesth. Intensive Care.* **2024**, *25*, 439–443. [CrossRef]
66. Pradniwat, P. Natural Products as Antioxidant Adjunct Therapy for Blood Parasitic Infections. In *Botanicals and Natural Bioactives: Prevention and Treatment of Diseases*; Bentham Science Publishers: Sharjah, United Arab Emirates, 2024; pp. 71–109.
67. Ashraf, M.V.; Khan, S.; Misri, S.; Gaira, K.S.; Rawat, S.; Rawat, B.; Khan, M.H.; Shah, A.A.; Asgher, M.; Ahmad, S. High-altitude medicinal plants as promising source of phytochemical antioxidants to combat lifestyle-associated oxidative stress-induced disorders. *Pharmaceuticals* **2024**, *17*, 975. [CrossRef] [PubMed]
68. Santos, P.H.S.; Suzuki, C.K.; Lannes, S.C.d.S. Effects of Adding Micronutrient Mixtures to a Model Dark Chocolate System and Partially Replacing the Fat Phase with a Structuring Oleogel. *Foods* **2025**, *14*, 430. [CrossRef] [PubMed]
69. Tumilaar, S.G.; Hardianto, A.; Dohi, H.; Kurnia, D. A comprehensive review of free radicals, oxidative stress, and antioxidants: Overview, clinical applications, global perspectives, future directions, and mechanisms of antioxidant activity of flavonoid compounds. *J. Chem.* **2024**, *2024*, 5594386. [CrossRef]

70. Banwo, O.G.; Popoola, D.O.; Achem, J.; Jeremiah, O.T. Evaluation of hematobiochemical and oxidative stress parameters in natural bovine *Trypanosoma brucei* infection. *Veterinaria* **2024**, *73*, 138–149. [CrossRef]
71. Fritzen, A.; de Vitt, M.G.; Deolindo, G.L.; Signor, M.H.; Correa, N.G.; Ribeiro, B.G.; Marques, J.; das Neves, G.B.; Miletti, L.C.; da Silva, A.S. Outbreak of *Trypanosoma vivax* in Dairy Cows: Hematologic, Immunological and Antioxidant Responses Before and After Treatment with Isometamidium Chloride. *Pathogens* **2025**, *14*, 143. [CrossRef]
72. Baldissera, M.D.; Souza, C.F.; Grando, T.H.; Moreira, K.L.; Schafer, A.S.; Cossetin, L.F.; da Silva, A.P.; da Veiga, M.L.; da Rocha, M.I.U.; Stefani, L.M. Nerolidol-loaded nanospheres prevent behavioral impairment via ameliorating Na+, K+-ATPase and AChE activities as well as reducing oxidative stress in the brain of Trypanosoma evansi-infected mice. *Naunyn-Schmiedeberg's Arch. Pharmacol.* **2017**, *390*, 139–148. [CrossRef]
73. Kristensson, K.; Mhlanga, J.; Bentivoglio, M. Parasites and the brain: Neuroinvasion, immunopathogenesis and neuronal dysfunctions. In *Protective and Pathological Immune Responses in the CNS*; Springer: Berlin/Heidelberg, Germany, 2002; pp. 227–257.
74. Matin, M.; Joshi, T.; Wang, D.; Tzvetkov, N.T.; Matin, F.B.; Wierzbicka, A.; Jóźwik, A.; Horbańczuk, J.O.; Atanasov, A.G. Effects of Ginger (*Zingiber officinale*) on the Hallmarks of Aging. *Biomolecules* **2024**, *14*, 940. [CrossRef]
75. Ayustaningwarno, F.; Anjani, G.; Ayu, A.M.; Fogliano, V. A critical review of Ginger's (*Zingiber officinale*) antioxidant, anti-inflammatory, and immunomodulatory activities. *Front. Nutr.* **2024**, *11*, 1364836. [CrossRef]
76. Vicidomini, C.; Palumbo, R.; Moccia, M.; Roviello, G.N. Oxidative Processes and Xenobiotic Metabolism in Plants: Mechanisms of Defense and Potential Therapeutic Implications. *J. Xenobiotics.* **2024**, *14*, 1541–1569. [CrossRef]
77. Zhou, L.; Zhang, J.; Zhao, K.; Chen, B.; Sun, Z. Natural products modulating MAPK for CRC treatment: A promising strategy. *Front. Pharmacol.* **2025**, *16*, 1514486. [CrossRef]
78. Qin, L.; Jiang, X.; Wei, Y.; Xie, J.; Yang, L. Effects of ginger root extract on cognitive impairment and the Nrf2/GPX4/SLC7A11 signaling pathway in aluminum-exposed rats. *Metab. Brain Dis.* **2025**, *40*, 1–14. [CrossRef]
79. Bahri, F.; Mansoori, M.; Vafaei, S.; Fooladi, S.; Mir, Y.; Mehrabani, M.; Hozhabri, Y.; Nematollahi, M.H.; Iravani, S. A comprehensive review on ginger-derived exosome-like nanoparticles as feasible therapeutic nano-agents against diseases. *Mater. Adv.* **2024**, *5*, 1846–1867. [CrossRef]
80. Famurewa, A.C.; Akhigbe, R.E.; George, M.Y.; Adekunle, Y.A.; Oyedokun, P.A.; Akhigbe, T.M.; Fatokun, A.A. Mechanisms of ferroptotic and non-ferroptotic organ toxicity of chemotherapy: Protective and therapeutic effects of ginger, 6-gingerol and zingerone in preclinical studies. *Naunyn Schmiedebergs Arch. Pharmacol.* **2024**, *398*, 4747–4778. [CrossRef]
81. Khoshnazar, S.M.; Mohagheghi, M.; Rahimi, S.; Dabiri, S.; Shahrokhi, N.; Shafieipour, S. Geraniol modulates inflammatory and antioxidant pathways to mitigate intestinal ischemia–reperfusion injury in male rats. *Naunyn Schmiedebergs Arch. Pharmacol.* **2025**, *398*, 8713–8727. [CrossRef]
82. Hofer, A. Targeting the nucleotide metabolism of *Trypanosoma brucei* and other trypanosomatids. *FEMS Microbiol. Rev.* **2023**, *47*, fuad020. [CrossRef]
83. Delespaux, V.; Geysen, D.; Majiwa, P.A.; Geerts, S. Identification of a genetic marker for isometamidium chloride resistance in Trypanosoma congolense. *Int. J. Parasitol.* **2005**, *35*, 235–243. [CrossRef]
84. Gupta, S.; Vohra, S.; Sethi, K.; Gupta, S.; Bera, B.C.; Kumar, S.; Kumar, R. In vitro anti-trypanosomal effect of ivermectin on *Trypanosoma evansi* by targeting multiple metabolic pathways. *Trop. Anim. Health Prod.* **2022**, *54*, 240. [CrossRef] [PubMed]
85. Ho, J.M.; Bakkalbasi, E.; Söll, D.; Miller, C.A. Drugging tRNA aminoacylation. *RNA Biol.* **2018**, *15*, 667–677. [CrossRef] [PubMed]
86. Ibba, M.; Söll, D. Aminoacyl-tRNA synthesis. *Annu. Rev. Biochem.* **2000**, *69*, 617–650. [CrossRef] [PubMed]
87. Kelly, P.; Hadi-Nezhad, F.; Liu, D.Y.; Lawrence, T.J.; Linington, R.G.; Ibba, M.; Ardell, D.H. Targeting tRNA-synthetase interactions towards novel therapeutic discovery against eukaryotic pathogens. *PLoS Neglected Trop. Dis.* **2020**, *14*, e0007983. [CrossRef]
88. Kim, S.; Yoon, I.; Son, J.; Park, J.; Kim, K.; Lee, J.-H.; Park, S.-Y.; Kang, B.S.; Han, J.M.; Hwang, K.Y. Leucine-sensing mechanism of leucyl-tRNA synthetase 1 for mTORC1 activation. *Cell Rep.* **2021**, *35*, 109031. [CrossRef]
89. Pham, J.S.; Dawson, K.L.; Jackson, K.E.; Lim, E.E.; Pasaje, C.F.A.; Turner, K.E.; Ralph, S.A. Aminoacyl-tRNA synthetases as drug targets in eukaryotic parasites. *Int. J. Parasitol. Drugs Drug Resist.* **2014**, *4*, 1–13. [CrossRef] [PubMed]
90. Nuryady, M.M.; Widayanti, R.; Nurcahyo, R.W.; Fadjrinatha, B. Characterization and phylogenetic analysis of multidrug-resistant protein-encoding genes in *Trypanosoma evansi* isolated from buffaloes in Ngawi district, Indonesia. *Vet. World* **2019**, *12*, 1573. [CrossRef] [PubMed]
91. Nuryady, M.M.; Nurcahyo, R.W.; Hindun, I.; Fatmawati, D. Multidrug resistance protein structure of *Trypanosoma evansi* isolated from buffaloes in Ngawi District, Indonesia: A bioinformatics analysis. *Vet. World* **2021**, *14*, 33. [CrossRef]
92. Ardelli, B.F. Transport proteins of the ABC systems superfamily and their role in drug action and resistance in nematodes. *Parasitol. Int.* **2013**, *62*, 639–646. [CrossRef]

93. Campos, M.C.; Phelan, J.; Francisco, A.F.; Taylor, M.C.; Lewis, M.D.; Pain, A.; Clark, T.G.; Kelly, J.M. Genome-wide mutagenesis and multi-drug resistance in American trypanosomes induced by the front-line drug benznidazole. *Sci. Rep.* **2017**, *7*, 14407. [CrossRef]
94. Da Costa, K.M.; Valente, R.d.C.; Fonseca, L.M.d.; Freire-de-Lima, L.; Previato, J.O.; Mendonça-Previato, L. The history of the abc proteins in human trypanosomiasis pathogens. *Pathogens* **2022**, *11*, 988. [CrossRef]